PNAS RESEARCH ARTICLE | BIOPHYSICS AND COMPUTATIONAL BIOLOGY

Experimentally determined leaflet–leaflet phase diagram of an asymmetric lipid bilayer

Thais A. Enoki[a,b,1,2] and Frederick A. Heberle[a,2]

Edited by Erwin London, Stony Brook University, Stony Brook, NY; received May 25, 2023; accepted October 11, 2023 by Editorial Board Member Lia Addadi

We have determined the partial leaflet–leaflet phase diagram of an asymmetric lipid bilayer at ambient temperature using asymmetric giant unilamellar vesicles (aGUVs). Symmetric GUVs with varying amounts of 1,2-dipalmitoyl-sn-glycero-3-phosphocholine and DOPC (1,2-dioleoyl-sn-glycero-3-phosphocholine) were hemifused to a supported lipid bilayer (SLB) composed of DOPC, resulting in lipid exchange between their outer leaflets. The GUVs and SLB contained a red and green lipid fluorophore, respectively, thus enabling the use of confocal fluorescence imaging to determine both the extent of lipid exchange (quantified for individual vesicles by the loss of red intensity and gain of green intensity) and the presence or absence of phase separation in aGUVs. Consistent with previous reports, we found that hemifusion results in large variation in outer leaflet exchange for individual GUVs, which allowed us to interrogate the phase behavior at multiple points within the asymmetric composition space of the binary mixture. When initially symmetric GUVs showed coexisting gel and fluid domains, aGUVs with less than ~50% outer leaflet exchange were also phase-separated. In contrast, aGUVs with greater than 50% outer leaflet exchange were uniform and fluid. In some cases, we also observed three coexisting bilayer-spanning phases: two registered phases and an anti-registered phase. These results suggest that a relatively large unfavorable midplane interaction between ordered and disordered phases in opposing leaflets (i.e., a midplane surface tension) can overwhelm the driving force for lateral phase separation within one of the leaflets, resulting in an asymmetric bilayer with two uniformly mixed leaflets that is poised to phase-separate upon leaflet scrambling.

asymmetric giant unilamellar vesicles | hemifusion | mismatch free energy | interleaflet coupling | registered and antiregistered phases

Significance

We report an experimentally determined phase diagram of an asymmetric lipid bilayer. We studied mixtures of a saturated and unsaturated lipid that separate into gel and fluid phases in symmetric bilayers. Consistent with theoretical predictions for strongly coupled bilayers, we found that increasing the concentration of unsaturated lipid in one of the leaflets abolished phase separation in the opposing leaflet. This scenario roughly mimics the phospholipid asymmetry of an animal cell plasma membrane, in which one leaflet contains a mixture of ordered and disordered lipids, while the other leaflet contains predominantly disordered lipids. Leaflet–leaflet phase diagrams reveal how cells can control membrane phase behavior by changing both the composition and asymmetric distribution of lipids.

Most cell membranes are asymmetric in their lipid composition. A striking example is the plasma membrane (PM) of animal cells, in which high-melting sphingomyelins (SMs) are found almost exclusively in the exoplasmic leaflet and lower-melting aminophospholipids (phosphatidylethanolamine and phosphatidylserine, PE and PS) are confined to the cytoplasmic leaflet (1). An ongoing challenge in biology is to elucidate the functional consequences for the cell of this lipid asymmetry, while a parallel challenge in biophysics is to establish its structural consequences for the membrane, including whether and how asymmetry influences the lateral organization of lipids within each leaflet (2). This phenomenon, often referred to as interleaflet coupling of phase behavior, is a crucial yet poorly understood aspect of the lipid raft hypothesis. The raft concept is typically defined in terms of favorable in-plane interactions between cholesterol (chol) and SM in the outer leaflet, which leads to their lateral segregation from more disordered phosphatidylcholine (PC) lipids (3). Because the inner leaflet lacks highly ordered SM or fully saturated glycerophospholipids and instead possesses mainly disordered unsaturated lipids, it is difficult to envision a role for rafts in signaling in the absence of a mechanism for strong interleaflet coupling whereby phase separation in the outer leaflet can induce segregation of inner leaflet lipids. Indeed, it is observed that some cytosolic acylated proteins, despite interacting only with the PM inner leaflet, nevertheless sense and respond to the organization of the outer leaflet (4–6), implying that outer leaflet physical properties are somehow "transmitted" across the bilayer.

Model membrane studies of symmetric bilayers have yielded important information about the phase behavior of compositions mimicking either the outer or inner PM leaflets. The former typically separate into coexisting liquid-disordered (*Ld*) and liquid-ordered (Lo) phases (7, 8), while the latter are invariably in a uniform *Ld* phase (9). For outer leaflet mixtures, the construction of ternary phase diagrams has greatly added to our understanding of how lipid and sterol structure influences the types of phases that can coexist and the location of phase boundaries (10). For organisms that regulate temperature, lipid composition is a key thermodynamic variable that could allow for control over membrane phase state (7), and compositional phase diagrams facilitate predictions for phases and phase transitions that could

Author contributions: T.A.E. and F.A.H. designed research; performed research; contributed new reagents/analytic tools; analyzed data; and wrote the paper.

The authors declare no competing interest.

This article is a PNAS Direct Submission. E.L. is a guest editor invited by the Editorial Board.

[1]Present address: Institute of Physics, University of Sao Paulo, Sao Paulo SP 05508-090, Brazil.

[2]To whom correspondence may be addressed. Email: ta327@cornell.edu or fheberle@utk.edu.

This article contains supporting information online at https://www.pnas.org/lookup/suppl/doi:10.1073/pnas.2308723120/-/DCSupplemental.

Published November 8, 2023.

be encountered (even transiently) when cells change the types of lipids found in their membranes (11).

In this regard, asymmetry is an additional thermodynamic degree of freedom that is relatively unexplored in the context of bilayer phase behavior; indeed, we are aware of no experimentally determined phase diagram for an asymmetric lipid bilayer. Despite a paucity of data, theorists have proposed leaflet–leaflet phase diagrams from mean-field models (12–15). In the simplest approach based on the Bragg-Williams approximation of regular solution theory, the free energy is governed by a competition between mixing entropy and the relatively unfavorable enthalpy of unlike lipid interactions; these are accounted for with a single parameter each for in-plane and out-of-plane interactions between unlike lipids. Minimizing the free energy over the full, asymmetric composition space results in predictions for the phase diagram of the mixture. The number and types of coexisting phases, and the locations of phase boundaries, depend strongly on the values of the interaction parameters, suggesting a rich phase behavior that could in principle be exploited by the cell through changing the composition and/or extent of asymmetry in the PM.

A major limitation to constructing compositional phase diagrams is the need to prepare and measure many mixtures. This is an especially high hurdle in the case of asymmetric bilayers, as existing methods for preparing asymmetric large unilamellar vesicles (LUVs) by cyclodextrin exchange are time-consuming, laborious, and low-throughput and result in a single ensemble-averaged measurement (i.e., one point on a phase diagram). Moreover, the phase state of these sub-micron-sized liposomes cannot be directly visualized with conventional microscopy and instead must be interrogated with indirect methods like fluorescence resonance energy transfer (FRET) (16–19) or neutron scattering (18, 20), though recent advances in cryogenic electron microscopy may eventually prove useful in this regard (21, 22). An alternative approach is the use of asymmetric giant unilamellar vesicles (aGUVs) prepared by calcium-induced hemifusion, in which the outer leaflet lipids of a conventionally prepared GUV are replaced with lipids from a supported bilayer after initiation of hemifusion between the two (23–28). It was previously found that the population of aGUVs from an individual hemifusion experiment has a broad distribution of asymmetry and thus a single experiment can provide data for multiple points within the asymmetric composition space (23). This proves to be extremely useful for the construction of leaflet-leaflet phase diagrams as we will show.

Here, we report an experimentally determined leaflet–leaflet phase diagram of a phospholipid mixture. We find many similarities with theoretical phase diagrams (13) that suggest relatively strong interleaflet coupling for our experimental system, DPPC (1,2-dipalmitoyl- sn-glycero-3-phosphocholine)/DOPC (1,2-dioleoyl-sn-glycero-3-phosphocholine) at room temperature. We discuss implications of the phase diagram for biological membranes.

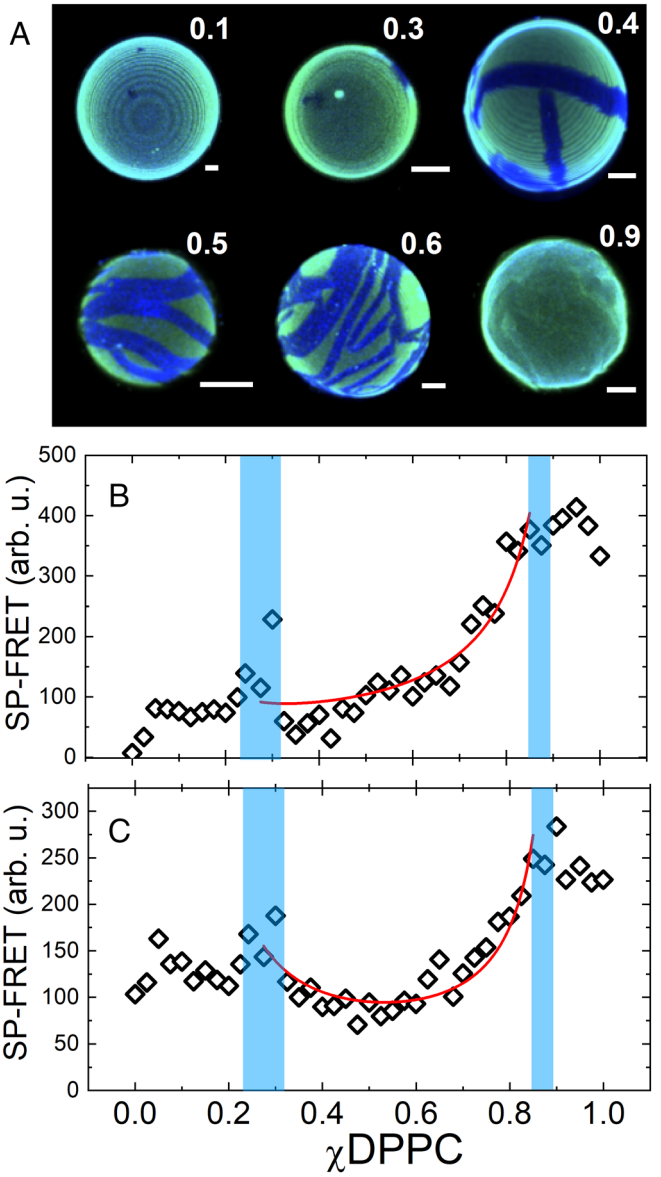

Fig. 1. Phase behavior of DPPC/DOPC symmetric bilayers at 22 °C. (*A*) confocal fluorescence maximum intensity projections of GUVs with increasing DPPC concentration as indicated (scale bar 5 μm.) GUVs were labeled with TFPC (green) and naphthopyrene (blue) which partition preferentially into *Ld* and *Lβ* phases, respectively. (*B* and *C*) FRET data for TOE donor to DHE acceptor (*Upper*) and DHE donor to TFPC acceptor (*Lower*). Each data point represents the ensemble-averaged signal of a single sample prepared by RSE as described in Methods. FRET efficiency is reduced in the *Ld*+*Lβ* coexistence region due to segregation of donor and acceptor, resulting in a U-shaped profile. The red curves are fits to Eq. **1**. Phase boundaries and probe partition coefficients are summarized in Table 1. The vertical blue bars mark the location and uncertainty of phase boundaries determined by visual inspection (see *SI Appendix* for details).

Results

Phase Behavior of Symmetric Bilayers. We first investigated the phase behavior of binary DPPC/DOPC mixtures in symmetric bilayers at ambient laboratory temperature (22 °C). Fig. 1*A* shows confocal projections of GUVs with different fractions of DPPC. The GUVs contained TopFluor-PC (TFPC) and naphthopyrene, which selectively partition into disordered and ordered phases, respectively (17, 19). GUVs with 10 mol% DPPC largely showed a uniform distribution of the probes, although occasional small domains enriched in naphthopyrene were observed (Fig. 1*A*). Increasing the mole fraction of DPPC resulted in a clear segregation of TFPC and naphthopyrene, consistent with the known partitioning behavior of these probes. The naphthopyrene-rich domains were typically elongated with irregular boundaries and grew in area fraction with increasing DPPC concentration. Vesicle shape also became increasingly nonspherical and faceted with increasing DPPC concentration, suggesting the presence of a rigid gel phase. At DPPC fractions, greater than 80%, yield was poor but the scant GUVs obtained had faceted shapes and a uniform distribution of both probes, consistent with a uniform *Lβ* phase.

We used a high-compositional resolution FRET assay to precisely determine the location of phase boundaries of symmetric DPPC/

DOPC bilayers at 22 °C. Fig. 1*B* shows FRET data for tryptophan oleoyl ester (TOE) donor to dehydroergosterol (DHE) acceptor (*Upper*) and DHE donor to TFPC acceptor (*Lower*) as a function of composition. The probe that is common to each pair, DHE, partitions favorably into the *Lβ* phase, while TOE and TFPC prefer the *Ld* phase. As a result, each trajectory exhibits a U-shaped region of reduced FRET efficiency marked by an abrupt decrease in signal at the onset of phase separation from either direction. The phase boundaries determined by visual inspection (Fig. 1 *B* and *C*, blue shaded regions) are in good agreement with boundaries determined from NMR (29). FRET data within the *Ld*+*Lβ* region were fit to Eq. **1** with probe partition coefficients as adjustable parameters, revealing good agreement with a simple tieline model (Fig. 1 *B* and *C*, solid red lines, Table 1). Because TFPC exhibits a large difference in its intrinsic fluorescence in *Ld* and *Lβ* phases (*SI Appendix*, Fig. S1), we were also able to separately extract its partition coefficient using Eq. **3**. We found similar values from these independent measurements, with Kp^{TFPC} = 10 ± 1 and 11 ± 1 from intrinsic fluorescence and FRET, respectively.

Phase Behavior of Asymmetric Bilayers. We then prepared asymmetric DPPC/DOPC GUVs (aGUVs) using calcium-induced hemifusion as previously described (23). Symmetric GUVs of varying DPPC/DOPC ratios were hemifused to a supported lipid bilayer (SLB) composed of DOPC, resulting in an overall increase in DOPC concentration (and corresponding decrease in DPPC concentration) within the outer leaflet of the aGUVs. The symmetric GUVs contained the far-red probe DiD to minimize energy transfer from the green probe TFPC that was included in the SLB. In symmetric DPPC/DOPC vesicles, DiD colocalized with NBD-DSPE [1,2-distearoyl-sn-glycero-3-phosphoethanolamine-N-(7-nitro-2-1,3-benzoxadiazol-4-yl)] which, like naphthopyrene, was brighter in the elongated domains with irregular boundaries, indicating that the long saturated chains of DiD confer preference for the gel phase (*SI Appendix*, Fig. S2). In contrast, TFPC prefers the fluid phase (Fig. 1*A* and *SI Appendix*, Fig. S2) and thus segregates from DiD in DPPC/DOPC bilayers.

The extent of asymmetry of individual aGUVs was quantified by the loss of red fluorescence and gain of green fluorescence as described in Materials and Methods. Fig. 2*A* plots the distribution of outer leaflet exchange percentage of individual aGUVs for four different initial compositions ranging from 10 to 60 mol% DPPC, the highest concentration for which we could successfully achieve hemifusion. Consistent with previous observations (23–26), exchange efficiency was highly variable, ranging from as low as 10% to ~100% of the outer leaflet. The phase state of individual aGUVs is also plotted in Fig. 2*A*, with open symbols indicating uniform vesicles and half-moon symbols indicating the presence of coexisting *Ld*+*Lβ* phases in the aGUV. As expected, GUVs that were in a uniform *Ld* phase prior to hemifusion (i.e., those with 10 mol% DPPC initially) remained uniform when the fraction of DOPC in their outer leaflets was further increased. In contrast, GUVs that were phase separated before hemifusion remained so only up to ~50% exchange of their outer leaflets. Moreover, the phase separated aGUVs with lower levels of exchange displayed irregular, faceted shapes (Fig. 2*C*) suggesting the presence of gel phase, while the uniform aGUVs with higher levels of exchange were smooth and spherical (Fig. 2*B*), suggesting a relatively fluid character in both leaflets.

Table 1. Probe partition coefficients obtained from FRET and intrinsic fluorescence data (*Kp* > 1 indicates preference for *Ld* phase)

Probe	FRET*		Intrinsic fluorescence†
	TOE to DHE	DHE to TFPC	
TOE	7 ± 1		
DHE	0.17 ± 0.03	0.2 ± 0.05	
TFPC		11 ± 1	10 ± 1

*data fit to Eq. **1**.
†data fit to Eq. **3**.

For phase-separated aGUVs, equatorial slices showed a pattern of alternating bright and dark for both DiD and TFPC intensities because of their distinct phase preference (*SI Appendix*, Fig. S3). An identical pattern was found in symmetric GUVs (*SI Appendix*, Fig. S3) and is consistent with phase registration, i.e., the opposing leaflets were either both relatively disordered (bright in the green channel and dim in the red channel) or both relatively ordered (dim in the green channel and bright in the red channel). In both symmetric and asymmetric GUVs, we also observed regions in which the intensities of the dyes was high, which could arise from domain antiregistration (i.e., a disordered domain in one leaflet opposite an ordered domain in the other leaflet). In symmetric GUVs, these small regions occurred exclusively near domain edges where intensities change rapidly. However, in aGUVs, we occasionally observed more extensive regions of probe colocalization, suggesting a true antiregistered (AR) phase in which the outer, TFPC-labeled leaflet was fluid and the inner, DiD-rich leaflet was gel (*SI Appendix*, Fig. S3). We caution that GUVs containing gel phases often show irregular shapes including "corners" of high curvature (e.g., Fig. 2*C*) that can potentially influence probe partitioning, thus precluding a precise quantitation of registered and AR phase fractions.

Uncertainty in Measured Outer Leaflet Exchange. We used a method based on maximum likelihood estimation (MLE) to determine the error in measured exchange, the full details of which are found in *SI Appendix*. Briefly, we first defined a *transition region* for each experimental trajectory, shown as boxes in Fig. 2*A*. The lower boundary of this region marks the highest value of exchange at and below which only phase separated vesicles were observed, while the upper boundary marks the lowest value of exchange at and above which only uniform vesicles were observed. The probability of observing m transition vesicles (red symbols in Fig. 2*A*) within this region is a function of the total number of observed vesicles N, the location of the true phase boundary ε^*, and the uncertainty in measured exchange fraction $\sigma_{\varepsilon_{app}}$, i.e., $Pr = Pr(m; N, \varepsilon^*, \sigma_{\varepsilon_{app}})$. We observed a phase boundary in three experimental trajectories (Fig. 2*A*) with: 1) N = 11, m = 0; 2) N = 11, m = 2; 3) N = 11, m = 3. Using ε^* = 0.6 and assuming the same exchange uncertainty for all aGUVs, the most likely value of $\sigma_{\varepsilon_{app}}$ is thus the one that maximizes the probability:

$$Pr \propto Pr\left(0; 11, 0.6, \sigma_{\varepsilon_{app}}\right) \times Pr\left(2; 11, 0.6, \sigma_{\varepsilon_{app}}\right) \times Pr\left(3; 15, 0.6, \sigma_{\varepsilon_{app}}\right).$$

We calculated this probability using simulated distributions in which $\sigma_{\varepsilon_{app}}$ was varied from 0.01 to 0.3, as shown in *SI Appendix*, Fig. S11. The uncertainty that maximizes the probability of our experimental observations is $\sigma_{\varepsilon_{app}} = 0.12$. This value was then used to calculate the uncertainty in composition of the aGUV outer leaflet through standard formulas for propagation of error (*SI Appendix*, Eq. **S3**), assuming a compositional uncertainty

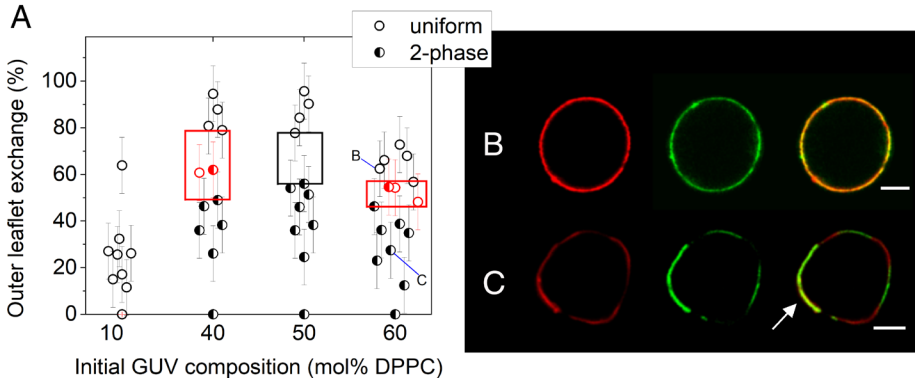

Fig. 2. Phase behavior of asymmetric DPPC/DOPC GUVs at 22 °C. (*A*) Distribution of outer leaflet exchange for aGUVs prepared from four different initial compositions. Each plotted data point represents a single aGUV. The phase state of the final aGUV is indicated by an open or half-filled symbol for uniform or phase-separated, respectively. Red boxes and symbols represent the transition region and transition vesicles, respectively, used to determine the uncertainty in measured exchange as described in the text and *SI Appendix* (we note that the data points at 0% exchange represent the initial symmetric GUV compositions and thus have no associated exchange uncertainty). (*B* and *C*) aGUVs formed from DPPC/DOPC 60/40 GUVs with either 62.5% (*B*) or 27.5% (*C*) outer leaflet exchange (compositions also marked in panel *A*). The arrow in *C* points to a region where order- and disorder preferring probes are colocalized, suggesting an antiregistered domain. (Scale bar 5 μm.)

for symmetric GUVs of 0.05. The compositions and errors are reported for individual aGUVs in Fig. 3 and *SI Appendix*, Tables S1–S4.

Interestingly, when the MLE error analysis was conducted separately for each probe (rather than using their average exchange), we found that the error in exchange fraction from DiD fluorescence ($\sigma^{DiD}_{\epsilon_{app}} = 0.18$) is greater than that calculated from TFPC fluorescence ($\sigma^{TFPC}_{\epsilon_{app}} = 0.12$). Propagation of these uncertainties implies an error for the average exchange fraction of $0.5 \times \sqrt{0.12^2 + 0.18^2} = 0.11$, a value that is very close to the value of $\sigma_{\epsilon_{app}} = 0.12$ that we obtained from applying the MLE method directly to the average exchange data.

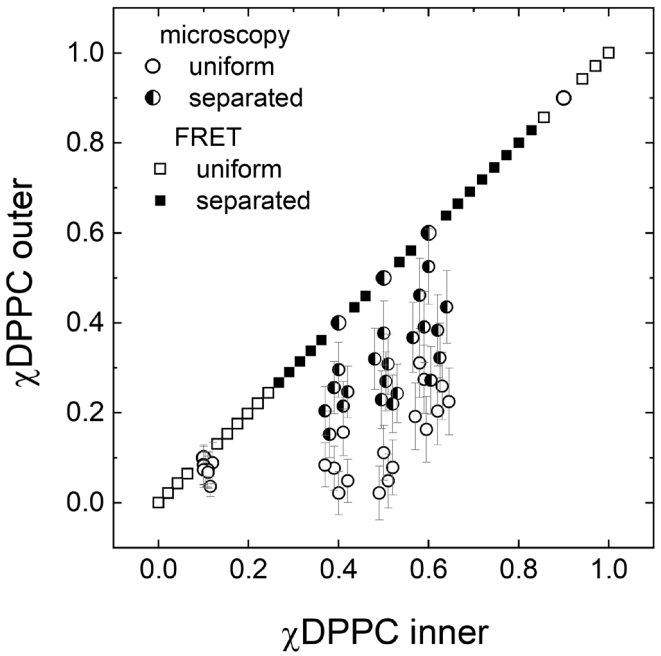

Fig. 3. Asymmetric phase diagram of DPPC/DOPC at 22 °C. Along the symmetric diagonal line, each plotted point represents the ensemble-averaged behavior of a single FRET sample (open or closed squares for uniform or phase-separated, respectively) or the dominant phase behavior of a population (N = 18 to 54) of symmetric GUVs (open or half-filled circles for uniform or phase-separated, respectively). All other plotted points represent the phase behavior of an individual aGUV (Fig. 2). Although the aGUV compositions fall on vertical (i.e., constant inner leaflet composition) trajectories, the corresponding data points in the figure are jittered horizontally for visibility.

Asymmetric Phase Diagram From Experimental Data. Fig. 3 shows FRET and microscopy data for all symmetric and asymmetric compositions plotted in a leaflet–leaflet phase diagram. The horizontal and vertical axes quantify the fraction of DPPC in the inner and outer leaflets, respectively; the diagonal line thus corresponds to symmetric compositions, while off-diagonal points correspond to asymmetric compositions. Assuming no lipid flip-flop during the time required to image samples postpreparation (~5 h), each hemifusion experiment corresponds to a vertical trajectory through the asymmetric composition space, originating on the diagonal (the initial symmetric GUV composition) and moving downward toward the horizontal axis as outer leaflet exchange proceeds; a vesicle whose outer leaflet was completely exchanged with DOPC from the SLB would lie at the end of the trajectory at $\chi_{DPPC\ outer} = 0$. The broad range of outer leaflet exchange observed in individual aGUVs (Fig. 2) results in the population of multiple points in the asymmetric composition space, each originating from a few experiments in which multiple GUVs undergo hemifusion (Fig. 3 circles) and thus facilitating the construction of a phase diagram.

Theoretical Leaflet-Leaflet Phase Diagrams. Leaflet–leaflet phase diagrams of asymmetric bilayers have been predicted using mean-field theories (12–15). We used a simplified theoretical approach employing a regular solution model with a single parameter each to describe in-plane and out-of-plane interactions between DPPC and DOPC, as described in Methods. Fig. 4*A* summarizes the salient details of the model, using an in-plane interaction parameter X = 2.25 and an out-of-plane interaction parameter Λ = 0.2 (both unitless) that are directly related to the lateral line tension and midplane surface tension, respectively (12). Three distinct bilayer-spanning phases are predicted: 1) a disordered-registered (DR) phase, in which lipids in both leaflets are relatively disordered; 2) an ordered-registered (OR) phase, in which lipids in both leaflets are relatively ordered; and 3) an AR phase characterized by low order in one leaflet and high order in the other. For our particular choice of interaction parameters, these phases can exist separately (white regions) or in coexistence: DR+OR (red shaded region), DR+AR (blue shaded region), OR+AR (green shaded region), or DR+OR+AR (gray shaded triangle). Within the two-phase

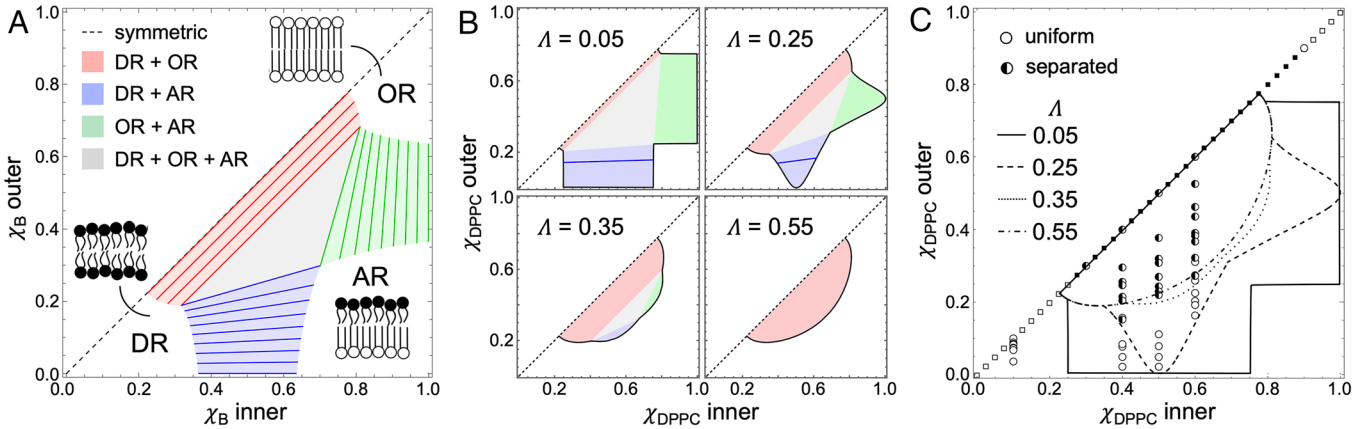

Fig. 4. Comparison of theoretical and experimental asymmetric phase diagrams. (A) Asymmetric phase diagram calculated from mean field theory with X = 2.25 and Λ = 0.2, as described in *Materials and Methods*. Schematic pictures show the three possible bilayer-spanning phases: DR, OR, and AR. Solid lines are tielines, gray-shaded region is a tie-triangle. (*B*) Phase diagrams for X = 2.25 and Λ increasing as indicated. (*C*) aGUV compositions showing phase-separated (half-filled circles) or uniform (open circles) are reproduced from Fig. 3 and overlaid with phase boundaries from Fig. 4*B*.

coexistence regions, several tielines are shown. For an idealized flat bilayer in the absence of asymmetric perturbations (e.g., a solid or cytoskeletal support, an applied electric or magnetic field, etc.), the phase diagram is mirrored across the diagonal (symmetric) line; we omit the upper half for simplicity.

Fig. 4*B* shows the influence of varying the interleaflet coupling parameter Λ at fixed X = 2.25. The fraction of the experimentally accessible composition space that is not in a phase coexistence region (i.e., the white regions, where aGUVs would appear uniform) increases with increasing Λ. In particular, the DR+AR arm of the phase diagram (blue shaded regions) shrinks and ultimately lifts off the horizontal axis when Λ > 0.25. As Λ approaches 0.55, the three-phase region closes to a single critical point, and the AR phase can no longer coexist with either registered phase. The single remaining phase-coexistence region for Λ > 0.55 is DR+OR (red shaded region in panel A), and its boundaries and tielines do not change with a further increase in Λ.

Fig. 4*C* shows an overlay of the phase coexistence boundaries from Fig. 4*B* and the experimental GUV and aGUV data from Fig. 3. The experimental data allow us to place limits on Λ in the DPPC/DOPC system: 1) a value of Λ < 0.35 is ruled out by the lack of phase-separated aGUVs below $\chi_{DPPC\ outer} = 0.2$; 2) the observation of AR phases at some compositions rules out values of Λ > 0.55.

Discussion

Experimental phase diagrams of symmetric bilayers containing two or three lipid components have provided valuable insights into lateral lipid interactions that contribute to the formation of lipid rafts in cell membranes (7, 8). Crucially, symmetric phase diagrams do not inform on transverse lipid interactions that can influence the lateral organization of asymmetric bilayers and thus may be important for understanding biological membranes that are often highly asymmetric. Mean-field theories have been used to predict leaflet–leaflet phase diagrams whose boundaries and phase regions are distinctive signatures of interleaflet coupling, but experimental phase diagrams of asymmetric bilayers have remained beyond reach due to the difficulty of generating asymmetric lipid distributions in synthetic vesicles. This situation has changed rapidly in recent years with the development of cyclodextrin-based methods for exchanging lipids between compositionally distinct vesicle pools (30–33), yet the first wave of studies utilizing these techniques have focused almost exclusively on preparing and characterizing highly asymmetric vesicles. In the context of a leaflet–leaflet phase diagram such as those shown in Fig. 4, this corresponds to a small subset of compositions near the horizontal axis. This approach to studying asymmetry sacrifices the wealth of information encoded in the locations of phase boundaries, and the number and type of coexistence regions. Moreover, most of these studies have utilized liposomes of submicron size which precludes measuring the asymmetry of individual vesicles.

Here, we have exploited a unique feature of the hemifusion method for preparing asymmetric GUVs that facilitates the construction of leaflet–leaflet phase diagrams: namely, the ability to assess the asymmetry and phase state of individual vesicles. It is fortuitous that the method produces a wide range of asymmetry as this allows us to populate multiple points on a phase diagram from a relatively small number of experiments.

Partial Leaflet–Leaflet Phase Diagram of DPPC/DOPC. We report what is to our knowledge the first experimentally determined leaflet–leaflet phase diagram for a lipid mixture (Fig. 3). We found that the region of coexisting registered *Ld*+*Lβ* phases found in symmetric DPPC/DOPC bilayers extends partially into the asymmetric composition space as outer leaflet DPPC is replaced by the more disordered lipid DOPC. Intriguingly, phase separation is observed only in aGUVs with lower levels of exchange: vesicles in which approximately half or more of the outer leaflet DPPC was replaced by DOPC during hemifusion consistently appear uniform and fully fluid (Fig. 2*B*). This observation suggests that the mismatch free energy—that is, the penalty for creating domains of an AR phase in which *Lβ* is directly opposite Ld—is so great as to induce complete mixing of DPPC and DOPC in the inner leaflet to minimize compositional differences (and thus, differences in order) across the bilayer once the level of outer leaflet exchange exceeds 50%. London has termed this outcome "disordered-leaflet dominance," in contrast to "separated-leaflet dominance" in which coexisting phases are observed even after one leaflet has been completely exchanged (or nearly so) with a more disordered lipid or lipid mixture (34).

Comparison to Theoretical Phase Diagrams and Estimate of the Mismatch Free Energy. The simplicity of a binary system invites a direct comparison with mean-field theories for asymmetric phase behavior (13). As shown in Fig. 4*C*, the experimentally determined asymmetric DPPC/DOPC phase diagram is at least superficially consistent with predictions from such theories. Specifically, values

of X ~ 2.25 and 0.35 < Λ < 0.55 result in phase boundaries that neatly delineate our observations of phase-separated and uniform aGUVs. This range of Λ corresponds to relatively strong interleaflet coupling in which the tendency of the DOPC-rich outer leaflet to be uniformly mixed dominates over the tendency of the inner leaflet composition to phase separate, resulting in completely uniform bilayers for aGUVs with higher levels of exchange. In the context of phase behavior, the common notion of interleaflet coupling strength thus maps directly to the free energy cost of forming domains of an AR phase in which highly ordered lipids in one leaflet are in direct contact with highly disordered lipids in the other leaflet.

We can estimate the mismatch free energy γ (in units of k_BT/nm^2) of an AR phase using the relationship $\gamma \approx \Lambda k_B T(\Delta\chi)^2 / a$, where $\Delta\chi$ is the inner/outer composition difference and a is the average molecular area (13). As discussed by May (12), γ is a midplane surface tension that effectively competes with the lateral line tension and thus can influence the partitioning of lipids in both leaflets (and consequently, their local order). The importance of the midplane surface tension for interleaflet coupling has been highlighted in recent perspective articles (35, 36). Using a = 0.55 nm^2 and taking the symmetric *Ld* and *Lβ* phase boundary compositions for X = 2.25 as a reference AR phase, we estimate that γ falls in the range of 0.2 to 0.3 k_BT/nm^2. These values are similar to a rough estimate of 0.5 k_BT/nm^2 based on an analogy with domain line tension (37), and a value of 0.1 to 0.2 k_BT/nm^2 calculated from MD simulations of ternary mixtures (38). Experimentally, Blosser et al. found that the energy required to deregister *Ld*+Lo domains in symmetric bilayers composed of DPPC/1,2-diphytanoyl-sn-glycero-3-phosphocholine/chol was 0.016 k_BT/nm^2 (39), an order of magnitude smaller than our estimate for the mismatch free energy of DPPC/DOPC aGUVs. It seems reasonable that a midplane interface between gel and fluid domains would be more unfavorable than that between two liquid phases, but this remains to be explored.

Type IA and IIA Phase Diagrams. Were the mismatch free energy much smaller than our estimated value of ~0.25 k_BT/nm^2, the penalty for the AR phase would be small and the phase boundaries of the symmetric bilayer (i.e., along the diagonal line) would extend nearly vertically to the horizontal axis (see, e.g., Fig. 4*B* with Λ = 0.05). In that case, all aGUVs formed from initially phase-separated GUVs would remain phase-separated as their outer leaflets were replaced with the more disordered lipid (even those approaching 100% replacement), and tielines in the DR+AR region would be nearly horizontal, reflecting essentially uniform mixing within the relatively disordered outer leaflet. In a scenario of slightly larger Λ (i.e., increased free energy cost of creating AR phase), the system now faces competing demands of maintaining lateral segregation of saturated and unsaturated lipids in the inner leaflet while simultaneously minimizing the impact of an ever-greater midplane surface tension within AR domains at higher levels of exchange. The compromise is to slightly *weaken* lateral segregation within the inner leaflet (quantified by the narrowing of phase boundaries of the DR+AR arm) and slightly *strengthen* lateral segregation within the outer leaflet (quantified by the increased tilt of DR+AR tielines). These changes in partitioning effectively reduce the difference in order of the gel and fluid leaflets of the AR domain: the gel phase becomes less ordered and the fluid phase becomes more ordered, thus lowering the midplane surface tension.

The regime of lower Λ just described (i.e., Λ < 0.25 for X = 2.25) corresponds to London's definition of separated-leaflet dominance (34), where coexisting phases are clearly present in highly asymmetric vesicles and lipids in the disordered leaflet—at a composition that would be uniformly mixed in symmetric bilayers—are instead partially segregated. This behavior has been observed experimentally in asymmetric vesicles: 1) in aGUVs prepared by hemifusion and composed of 1,2-distearoyl-sn-glycero-3-phosphocholine (DSPC)/DOPC/Chol, where initially symmetric GUVs with *Ld*+Lo domains remained visually phase separated even after nearly all of the outer leaflet DSPC was replaced with DOPC/Chol (at similar chol fraction as the inner leaflet), and a dye localized to the outer leaflet showed nonuniform partitioning between the domains (23); 2) in visually phase separated aGUVs where egg-SM was introduced into the outer leaflet of DOPC/Chol GUVs by cyclodextrin, and an order-preferring dye localized to the inner leaflet colocalized with an order-preferring dye in the outer leaflet (40). A similar behavior has also been reported in asymmetric SLBs (41) and planar bilayers (42). Furthermore, the disordering of outer leaflet DPPC-rich gel domains opposite a fluid 1-palmitoyl-2-oleoyl-sn-glycero-3-phosphocholine (POPC) leaflet has been observed in asymmetric LUVs and is likely explained by weakened segregation of DPPC and POPC in the outer leaflet (43). To summarize, previous observations in asymmetric bilayers of both induced order in the leaflet enriched in unsaturated lipids, and induced disorder in the leaflet enriched in saturated lipids, can be understood in terms of the interplay between line tension and midplane surface tension.

Returning to Fig. 4, values of Λ > 0.25 cause the DR+AR phase region to lift off the horizontal axis until eventually, at Λ > 0.55, AR and DR phases can no longer coexist. In this regime, only a single coexistence region of registered phases (DR+OR) remains, and only at lower levels of asymmetry; higher levels of asymmetry result in a uniform asymmetric phase (discussed further in the next section). This behavior has also been reported in asymmetric planar bilayers (42) and in asymmetric LUVs composed of saturated PC/DOPC/Chol, when the chain length of the high-melting saturated PC lipid was 14, 15, or 16 carbons (34).

Our findings here, together with experimental observations mentioned above, imply that the full range of phase diagram morphologies demonstrated in Fig. 4*B* may be experimentally accessible in simple 2- and 3-component mixtures of phospholipids and chol. This suggests a need for updated nomenclature to classify these systems and facilitate their comparison. In analogy to the Type I/Type II notation introduced by Feigenson (44), where I and II refer to the number of macroscopic coexisting phases at high chol concentrations, we suggest Type IA/Type IIA to refer to asymmetric phase diagrams in which either one (Type IA) or two (Type IIA) macroscopic phases are observed in highly asymmetric vesicles. Thus, phase diagrams in Fig. 4 with Λ < 0.25 would result in Type IIA behavior and those with Λ > 0.25 would result in Type IA behavior. As mentioned above and noted previously by Williamson and Olmsted (15), this classification scheme maps directly to London's coupling dominance model (34), with Type IA and Type IIA behavior corresponding to disordered-leaflet dominance and separated-leaflet dominance, respectively.

The Uniform Asymmetric Phase Is a Unique State of Matter. As mentioned previously, Wang and London (34) reported suppression of *Ld*+Lo phase separation in saturated PC/DOPC/Chol asymmetric vesicles when the chain length of the saturated PC was 16 carbons or shorter (34). We report here a similar observation of uniformly mixed bilayers formed by DPPC/DOPC aGUVs at higher levels of exchange (i.e., Type IA behavior). The uniform asymmetric "phase" is a quasiequilibrium state that exists only in asymmetric bilayers at time scales much shorter than lipid flip-flop, which occurs with a halftime of several days in liposomes at room temperature (45). In this unique state of matter, the more ordered leaflet, though well-mixed, has a composition that is thermodynamically unstable in isolation and would separate into

coexisting ordered and disordered phases in a symmetric bilayer. It is prevented from demixing in the asymmetric bilayer only by the free energy cost of creating a highly ordered domain (in our case, a DPPC-rich *Lβ* domain) that must then share a high-energy interface with a disordered *Ld* phase in the opposite leaflet. The uniform asymmetric phase is essentially unexplored in membrane structural biology; a thorough characterization of its structural and mechanical properties may yield important insights into the behavior of cellular PMs.

While our experiments say little about the biophysical properties of the uniform asymmetric phase, it is notable that these aGUVs appear spherical rather than faceted (Fig. 2*B*), suggesting that the inner leaflet has a fluid rather than gel-like character despite its relatively high DPPC concentration. A similar observation was obtained from neutron scattering experiments of asymmetric LUVs prepared by cyclodextrin exchange of DPPC into POPC vesicles, where approximately one-third of the outer leaflet POPC was replaced by DPPC (43). Importantly, POPC vesicles are slightly more ordered than DOPC vesicles. While the scattering data in that study were consistent with coexisting ordered+disordered environments in the outer leaflet (in contrast to the fully uniform vesicles observed here), the DPPC-rich ordered phase had a markedly lower area per lipid and thickness than typical gel phases, suggesting partial fluidization due to the influence of the disordered POPC-rich leaflet. It remains to be seen whether the uniform asymmetric phases observed here are heterogeneous on submicron length scales.

Implications for Biological Membranes. Our experimental system attempts to mimic the difference in order between outer and inner leaflets of mammalian PM, with three major differences. First, in our system, the inner leaflet contains a mixture of low-melting and high-melting lipids (similar to the PM outer leaflet) and our outer leaflet becomes progressively more disordered with increasing levels of exchange (similar to the PM inner leaflet). Second, the aGUVs in our study contain no chol, a major component of animal cell PM. Third, because of the lack of chol, the ordered phase in our aGUVs is gel (*Lβ*), as opposed to the Lo phase found in the PM. Because of these differences, we are cautious about extrapolating our findings to biological membranes. However, observations in chol-containing aGUVs with coexisting *Ld*+Lo phases (discussed in the previous sections) suggest that both Type IA and Type IIA behaviors may be biologically relevant, depending on the types of lipids present in the bilayer and the extent of their asymmetry. A corollary is that cells may have the ability to tune phase boundaries and the types of bilayer-spanning phases present (i.e., registered or anti-registered) by changing the composition and/or asymmetric distribution of PM lipids. We now speculate on a few such possibilities.

As one example, phase diagrams enable predictions for how changes in membrane composition that influence PM inner or outer leaflet order can in turn alter biological domains such as lipid rafts. For example, lipids or exogenous molecules that localize to domain interfaces (i.e., linactants) can reduce the energy penalty associated with in-plane contacts between order-preferring and disorder-preferring lipids, thus narrowing the size of the miscibility gap in which multiple bilayer-spanning phase can coexist (equivalent to lowering the value of X in the mean field model). On the other hand, any molecule that partitions favorably to the bilayer midplane would lower Λ and expand the miscibility gap, possibly also creating AR phases. Such midplane partitioning might be favorable for small hydrophobic molecules and has been observed experimentally for short-chain alkanes (46) and even chol (47, 48). Importantly, the number and types of bilayer-spanning phases are governed by a competition between in-plane and out-of-plane interactions embodied by X and Λ in the mean field theory. Any change in the composition of either leaflet can in principle alter the balance of these interactions and change the underlying phase diagram.

Another, distinct way of traversing the asymmetric phase space involves the action of lipid translocases (i.e., flippases, floppases, or scramblases). Translocase activity alters the distribution of lipids between leaflets while maintaining fixed overall bilayer composition. In the context of a leaflet–leaflet phase diagram, this corresponds to movement along trajectories perpendicular to the symmetric diagonal which—depending on the pre-flip-flop composition—can result in phase transitions (15). Phase diagrams like those shown in Fig. 4*C* thus offer a potential explanation for numerous observations of macroscopic liquid phase coexistence in giant PM vesicles (GPMVs), but not in the parent cells from which they were derived (49–53). Although quantitative data are scarce, GPMV permeability to hydrophilic solutes suggests at least partial if not complete loss of asymmetry during the blebbing process (54). Assuming a highly asymmetric initial composition for the PM of the resting cell (i.e., a location in the lower right portion of the phase diagram), scrambling corresponds to movement up and to the left (i.e., toward the symmetric diagonal) and—depending on the extent of scrambling—across a phase boundary, resulting in the formation of large domains. It was recently reported that GMPVs produced by N-ethyl maleimide (NEM) treatment retain more asymmetry than those produced by dithiothreitol/paraformaldehyde treatment (55). Intriguingly, the same study also found that NEM-induced GPMVs showed enhanced domain stability after their asymmetry was destroyed, further supporting the hypothesis that rafts in native cells may be suppressed by strong interleaflet coupling but poised for formation upon scrambling. This mechanism may also be relevant to the normal function of healthy, nonapoptotic cells, as it is increasingly clear that transient and reversible loss of asymmetry can be associated with intercellular communication and intracellular signaling events (56).

Flip-Flop in Asymmetric GUVs. The aGUV data reported in this study were collected within 5 h of aGUV preparation to minimize flip-flop. Although we did not directly assay for flip-flop, we note that in previous studies, aGUVs prepared by hemifusion have been shown to retain their asymmetry for at least several hours postpreparation as evidenced by nearly complete dithionite quenching of the dye that was introduced into the outer leaflet (23). Along similar lines, Steinkühler et al. used dithionite quenching to demonstrate a highly asymmetric distribution of NBD-PG in GUVs 1 h after electroformation, with a substantial (though not complete) loss of probe asymmetry after 26 h (57). While the dye is itself a unique component of the system with a flip-flop rate that is potentially different from the host lipids, direct measurements of DPPC and POPC flip-flop rates by proton NMR also suggest that flip-flop should be minimal over the course of several hours at room temperature (43, 45).

Uncertainty in Measured Exchange of aGUVs. We found that the error in exchange fraction is 1.5-fold greater when calculated from DiD fluorescence compared to TFPC fluorescence ($\sigma_{\epsilon_{app}}^{DiD} = 0.18$, $\sigma_{\epsilon_{app}}^{TFPC} = 0.12$). It is not clear if this is due to differences in probe photophysical properties (e.g., brightness, photostability) or to potentially different sources of error for the two probes. The latter might be expected, given that their role in the experiment is very different: DiD is incorporated into the electroformed GUVs and exits the GUV during hemifusion, while TFPC is incorporated into the SLB and enters the GUV during hemifusion. It is notable that, were the error in DiD exchange only slightly greater (√3-fold larger than that of TFPC, or 0.21), there would be no advantage to averaging the

two measurements, since the value derived from TFPC alone would have greater precision than the mean. Further investigation of the sources of uncertainty and how they propagate for these and other probes will undoubtedly lead to improved accuracy of measured aGUV composition.

Compositional Uncertainty of aGUVs. The error in aGUV outer leaflet composition (calculated by propagating the uncertainty of the exchange measurement using *SI Appendix*, Eq. **S3**) ranges from 0.022 to 0.084 in DPPC mole fraction, depending on both the initial DPPC concentration prior to exchange and the amount of outer leaflet exchange (Fig. 3). For a given fraction of exchanged lipid, uncertainty increases with initial DPPC concentration, while for a given initial DPPC concentration, uncertainty decreases with increasing fraction of exchange (*SI Appendix*, Tables S1–S4).

The uncertainties we report, based on a maximum likelihood estimation, suggest that the compositional variability of individual aGUVs prepared by hemifusion is in some cases larger than previously appreciated. One complicating factor when gel phases are present is the effect of a nonspherical vesicle shape on the measured fluorescence intensity values used to quantify exchange. This results in greater pixel-to-pixel variation in intensity that in turn propagates into the compositional error and as such is reflected in the larger uncertainties we report here. A rigorous error analysis would need to account for these effects, as well as uncertainty introduced by a host of other factors including probe partitioning and variability in the average fluorescence of GUVs prior to hemifusion. Such a treatment is beyond the scope of this study but is the subject of ongoing investigation by our groups. We instead chose here to estimate the uncertainty directly from the data, i.e., using the observation of transition vesicles to infer the underlying distribution which is itself a function of the compositional uncertainty. This method in principle captures all contributing sources of random error while minimizing assumptions.

Importantly, our primary result—namely, the observation of a phase boundary in the asymmetric composition space, and its implications for interleaflet coupling—is not obscured by the compositional uncertainty of individual aGUVs due to the large number of vesicles that were analyzed ($N = 45$) and their broad compositional coverage. This claim is further supported by simulated replicate experiments with similar noise (*SI Appendix*, Fig. S8), each of which still clearly shows the presence of a phase boundary.

Summary and Outlook

We have determined what is to our knowledge the first leaflet–leaflet phase diagram for an asymmetric lipid bilayer that roughly mimics the difference in leaflet order of an animal cell PM. We used asymmetric GUVs prepared by hemifusion, which resulted in a broad distribution of asymmetric compositions that facilitated the construction of a phase diagram. In aGUVs with less than 50% outer leaflet exchange, we find as many as three distinct types of bilayer-spanning phases in coexistence: a registered ordered phase, a registered disordered phase, and in some cases an AR phase characterized by a relatively disordered outer leaflet and a relatively ordered inner leaflet. In contrast, vesicles with greater than 50% exchange appeared uniform, suggesting a high energy penalty for the creation of AR phase at these compositions. The system instead responded by abolishing phase separation entirely, an outcome consistent with previous reports of "uniform leaflet dominance" in asymmetric liposomes (13). A key takeaway is that symmetric phase diagrams cannot be relied upon to infer the phase behavior of an asymmetric bilayer, because lateral organization of lipids in both leaflets can be dramatically altered by unfavorable interleaflet interactions.

Our results highlight the utility of a physical chemistry-based approach for studying the mixing behavior of complex, asymmetric biological membranes. In particular, an experimental phase diagram combined with simple mean field theory provides an intuitive framework for understanding how leaflet phase behavior is coupled in asymmetric membranes, and predicting how such membranes might respond to perturbations in leaflet composition. Still, obvious limitations exist. We chose a binary phospholipid mixture (rather than a more biologically relevant chol-containing ternary mixture) precisely because experimental observations could be straightforwardly mapped to the asymmetric composition space and thus, easily compared to theoretical predictions. The addition of chol is more complicated still, as it rapidly samples not only coexisting environments within a given leaflet, but also the two leaflets themselves due to its intrinsically faster rate of flip-flop. For chol-containing ternary mixtures, one possibility is to ensure that chol's chemical potential remains constant throughout the composition space, allowing it to be omitted from the phase diagram entirely. This could be achieved by matching chol's chemical potential in the symmetric phase separated GUVs and the supported bilayer used for hemifusion. The symmetric diagonal of the phase diagram would thus correspond to a symmetric *Ld*+Lo tieline. Such an experiment should be feasible given recent reports that chol chemical potential can be measured in synthetic liposomes (58).

Materials and Methods

Chemicals. DPPC and DOPC were purchased from Avanti Polar Lipids (Alabaster, AL, USA). Chol was obtained from Nu Chek Prep. HEPES [4-(2-hydroxyethyl)-1-piperazineethanesulfonic acid], NaCl (sodium chloride), $CaCl_2$ (calcium chloride), EDTA (ethylenediaminetetraacetic acid), and sucrose were from Sigma-Aldrich (St. Louis, MO, USA). Phospholipids were dissolved in chloroform to prepare working stock solutions, the concentrations of which were determined to within 1% using an inorganic phosphate assay (26). Lipid purity was determined to be > 99% using thin-layer chromatography (TLC); ~20 μg of lipid was diluted in chloroform and spotted onto prewashed, activated silica gel GHL plates (Analtech) and subsequently developed with chloroform/methanol/water (65/25/4). Chol stock purity was checked with TLC in petroleum ether/diethyl ether/chloroform (7/3/3).

Fluorescent dyes ergosta-5,7,9(11),22-tetraen-3β-ol (DHE, Sigma-Aldrich), NBD-DSPE (Avanti), 1-palmitoyl-2-(dipyrromethemeboron difluoride)undecanoyl-sn-glycero-3-phosphocholine (TFPC, Avanti), 1,1′-dioctadecyl-3,3,3′,3′-tetramethylindodicarbocyanine, 4-chlorobenzenesulfonate salt (DiD, ThermoFisher Scientific, Waltham, MA), naphtho[2,3-a]pyrene (naphthopyrene, Tokyo Chemical Industry Co., Tokyo, Japan), and TOE (synthesized in the laboratory of Erwin London) were prepared as stock solutions in chloroform. The concentration of dyes diluted in methanol was measured with absorbance spectroscopy. Excitation coefficients were 12,900 $(M\,cm)^{-1}$ at 324 nm for DHE; 23,749 $(M\,cm)^{-1}$ at 454 nm for naphthopyrene; 91,800 $(M\,cm)^{-1}$ at 504 nm for TFPC; 270,000 $(M\,cm)^{-1}$ at 644 nm for DiD; 21,000 $(M\,cm)^{-1}$ at 466 nm for NBD-DSPE; and 5,500 $(M\,cm)^{-1}$ at 280 nm for TOE. We also confirmed purity of the dye stocks as >99% using TLC.

Sample Preparation for Fluorescence Spectroscopic Measurements. Samples for fluorescence spectroscopic measurements were prepared by rapid solvent exchange (RSE) (59). Lipids and dyes dissolved in chloroform were dispensed into 13 × 100 mm glass tubes with FEP-lined screw caps using a 25-μL glass syringe attached to a repeating dispenser (Hamilton Co.). A 0.5 mL aliquot of aqueous buffer (5 mM PIPES [piperazine-N,N′-bis(2-ethanesulfonic acid)], 200 mM KCl, 1 mM EDTA, pH 7.0) was added to the tube, which was then placed under vacuum for 1 min while vortexing. This procedure rapidly removes the chloroform and results in fully hydrated bilayers containing one to a few lamellae (36). Samples were sealed with argon and placed in a water bath at 55 °C, then slowly cooled to 22 °C at a rate of 1.4 °C/h. In this manner, trajectories with 41 total samples of varying composition (χDPPC ranging from 0 to 1), each with a fixed concentration of TOE (1/100 probe/lipid), DHE (1/100), and TFPC (1/1,500) were prepared. The three probes constitute two FRET pairs: TOE donor to DHE acceptor, and DHE donor to TFPC acceptor.

Fluorescence Measurements. Fluorescence intensity was measured with a spectrofluorimeter model F7000 (Hitachi High Technologies America, Schaumburg, IL) equipped with a high-sensitivity cell holder using excitation and emission slit widths of 5 nm and integration time of 10 s. Additionally, light scattering was monitored by setting both the excitation and emission wavelength to 400 nm. We used the following excitation and emission wavelengths to measure the intensity of individual probes: TOE, $\lambda_{ex}/\lambda_{em}$ = 284/335 nm; DHE, $\lambda_{ex}/\lambda_{em}$ = 327/393; and TFPC, $\lambda_{ex}/\lambda_{em}$ = 500/520 nm. FRET was measured as sensitized acceptor emission upon donor excitation using the following wavelength combinations: TOE/DHE, $\lambda_{ex}/\lambda_{em}$ = 284/393; and DHE/TFPC, $\lambda_{ex}/\lambda_{em}$ = 327/520 nm.

FRET Data Analysis. FRET trajectories were fit with the equation

$$FRET(f_{L\beta}) = \frac{F_{Ld}K_p^D K_p^A(1-f_{L\beta}) + F_{L\beta}f_{L\beta}}{\left[K_p^A + (1-K_p^A)f_{L\beta}\right]\left[K_p^D + (1-K_p^D)f_{L\beta}\right]}, \quad [1]$$

where K_p^D and K_p^A are the partition coefficients of the FRET donor and acceptor, respectively (with $K_p > 1$ indicating preference for the *Ld* phase), F_{Ld} and $F_{L\beta}$ are the observed FRET values at the compositions marking the *Ld* and *Lβ* tieline endpoints at compositions χ_{DPPC}^{Ld} and $\chi_{DPPC}^{L\beta}$, respectively, and $f_{L\beta}$ is the mole fraction of gel phase present at the phase-separated composition χ_{DPPC}, given by the lever rule:

$$f_{L\beta} = \frac{\chi_{DPPC} - \chi_{DPPC}^{Ld}}{\chi_{DPPC}^{L\beta} - \chi_{DPPC}^{Ld}}. \quad [2]$$

Tieline endpoints were determined from the trajectory by visual inspection as compositions where FRET changed abruptly. Moreover, K_p of TFPC was independently measured in single-dye fluorescence experiments described below, allowing us to determine K_p of the second dye from fitting FRET data to Eqs. **1** and **2** using a single free parameter.

Single Dye Fluorescence to Determine Probe Partition Coefficients. Sample trajectories were prepared as described in the previous section except that here, a single fluorescent dye (TFPC) was used at a probe/lipid ratio of 1/1,500. The fluorescence intensity of TFPC is sensitive to its local environment; specifically, it is markedly dimmer in the gel phase compared to the *Ld* phase, thus providing a handle for measuring its partitioning between these phases (19). Fluorescence intensity *I* as a function of gel phase mole fraction $f_{L\beta}$ was fit with the equation

$$I\left(f_{L\beta}\right) = \frac{I_{Ld}K_p(1-f_{L\beta}) + I_{L\beta}f_{L\beta}}{K_p + (1-K_p)f_{L\beta}}, \quad [3]$$

where I_{Ld} and $I_{L\beta}$ are the observed fluorescence intensity values at the compositions marking the pure *Ld* and *Lβ* tieline endpoints and all other parameters are as previously defined. Thus, with the knowledge of the phase boundaries, we used Eq. **3** to determine the K_p of TFPC (Fig. 2).

Preparation of GUVs. GUVs were prepared by electroformation as previously described (60). Briefly, a mixture of lipids and DiD (1/2,500 probe/lipid) diluted in chloroform was spread onto the ends of two indium tin oxide-coated glass microscope slides (Delta Technologies, Loveland, CO). Residual chloroform was removed by placing the slides in a heated chamber attached to a vacuum pump; the chamber was maintained at low pressure and 45 °C for 2 h. A sandwich was formed from the two slides using an O-ring spacer filled with 100 mM sucrose solution and placed into an aluminum holder heated to 50 °C. GUVs were formed by applying a 1 V peak-to-peak, 5 Hz waveform to the sandwich for 2 h while the holder was maintained at 50 °C, followed by slow cooling to 22 °C at a rate of 1.4 °C/h. GUVs were harvested from the chamber and stored in plastic microfuge tubes prior to imaging.

Preparation of SLBs. SLBs were prepared by vesicle deposition. First, paucilamellar vesicles composed of DOPC with trace TFPC (1/1,500 dye/lipid ratio) were prepared using the RSE procedure described above. The sample volume of 1.2 mL (2.5 mM total lipid concentration) was then divided into two 0.6 mL samples that were separately sonicated for ~20 min in a circular bath sonicator (Sonblaster, Narda Ultrasonics Co., Mineola, NY). The initial RSE samples were visibly cloudy, but sonicated samples appeared transparent, indicating the formation of small unilamellar vesicles (SUVs). The two SUV samples were then combined and diluted with an equal volume of 1 M NaCl solution before aliquoting into a four-well Lab-Tek II chambered cover glass dish (Thermo Fisher Scientific) that had been treated with 1 M KOH, copiously rinsed with Milli-Q water, and plasma cleaned as previously described (23). The SUV solution was added to the dish and held at 4 °C for 2 h to form the SLB. To remove lipid aggregates attached to the SLB surface, the dish was immersed in a 2-L beaker filled with Milli-Q water and a plastic 10 mL syringe was used to gently flush each well. Surface coverage and lipid mobility were assessed with FRAP prior to subsequent hemifusion experiments.

Preparation of aGUVs by Hemifusion. Asymmetric GUVs were prepared as previously described (23). Briefly, 20 to 25 μL of symmetric GUVs were added to the SLB chamber in 5 μL aliquots. After sufficient time to allow the GUVs to settle by gravity and establish close contact with the SLB, a Ca^{2+}-containing buffer (HEPES 25 mM, NaCl 25 mM, $CaCl_2$ 10 mM, pH 5, 103 mOsm/kg) was added to initiate hemifusion. Hemifusion was monitored with confocal microscopy, as the lipids and fluorophore (TFPC) initially in the SLB diffused into the GUV outer leaflet and were replaced by lipids and fluorophore (DiD) initially in the GUV. After 20 to 30 min, EDTA was added to chelate Ca^{2+} and prevent further fusion, and aGUVs were detached from the SLB by gentle pipet mixing.

Observation of GUVs with Confocal Microscopy. Images of GUVs were collected with a Nikon Eclipse C2+ laser scanning confocal microscope equipped with a Plan Apo VC 60× A WI DIC N2 objective and NIS-Elements Basic Research software (Nikon Instruments, Melville, NY). A one-way scan direction was used with scan speed set to 0.5. TFPC and DiD were excited with 488 nm and 640 nm laser lines at 7% and 10% laser power (scale 0 to 100%), respectively. For both probes, the gain was 85 (scale 0 to 255) and the offset was 0. Polarization artifacts were corrected by inserting a quarter wavelength plate (Thermo Fisher Scientific) into the excitation path as previously described (23).

Estimating Lipid Exchange from Dye Intensity Measurements. Fluorescence intensity profiles *I vs.* θ were calculated from confocal slices at the equators of GUVs and aGUVs using built-in routines in ImageJ and Mathematica as previously described (23). The total intensity was also calculated by summing the intensity for all angles θ = 0 to 360°. The percentage of lipid exchange *P* was then calculated for each individual aGUV by comparing its total intensity to the average intensity measured in a set of symmetric control GUVs containing only TFPC or DiD at their respective initial concentrations of 1/1,500 and 1/2,500. Each probe thus provides an independent estimate of percent exchange, calculated as

$$P_{TFPC} = 2\frac{I_{aGUV}}{I_{GUV}} \times 100\,\%, \quad [4]$$

$$P_{DiD} = 2\left(1 - \frac{I_{aGUV}}{I_{GUV}}\right) \times 100\,\%, \quad [5]$$

where $\langle I_{GUV} \rangle$ is the average intensity of the set of symmetric control GUVs and I_{aGUV} is the intensity of an aGUV. As in previous studies using the hemifusion method (23), we considered only vesicles in which the percentage of lipid exchange calculated from TFPC and DiD agreed to within 20%. Indeed, a large disagreement would be expected in the event of multiple lamellae or full fusion, and the 20% criterion thus serves to filter out vesicles that are likely to harbor artifacts.

The error in P_{TFPC} and P_{DiD} was determined from a maximum likelihood method described briefly in *Results* and in detail in *SI Appendix*. We used the average of P_{TFPC} and P_{DiD} to estimate the outer leaflet lipid composition of the aGUV,

$$\chi_{DPPC,out}^{aGUV} = (1 - P/100)\chi_{DPPC}^{GUV}, \quad [6]$$

assuming that the rate of exchange of lipids is equal to that of the probes. In Eq. **6**, χ_{DPPC}^{GUV} is the initial composition of the symmetric GUV prior to hemifusion, and *P* represents the mean value calculated from P_{TFPC} and P_{DiD}. Error in the lipid composition of the outer leaflet, $\chi_{DPPC,out}^{aGUV}$, was estimated by propagating the uncertainty in P_{TFPC} and P_{DiD} using *SI Appendix*, Eq. **S3**.

Theoretical Asymmetric Phase Diagrams. We used a previously described mean-field theory to calculate asymmetric phase diagrams (13). Briefly, the phase regions of an asymmetric binary A-B mixture are controlled by dimensionless parameters $\mathbf{X}$ and Λ that quantify nonideal in-plane and out-of-plane interactions of the

lipids, respectively. X embodies the effective strength of nearest-neighbor interactions and thus describes the nonideality of the mixture; a large, positive value of X increases the extent of the miscibility gap along the diagonal line of the phase diagram as shown in Figs. 3 and 4. Λ embodies the coupling strength between the two leaflets, penalizing differences in their order; a large, positive value of Λ implies a high energy cost of maintaining distinct phases in opposing leaflets. X and Λ are thus directly related to the lateral line tension and midplane surface tension, respectively, and the phase boundaries and phase regions in the leaflet-leaflet phase diagram represent a compromise between their competing tendencies (12).

Phase boundaries were calculated by minimizing the local free energy of the bilayer,

$$f_B\left(\chi_{DPPC}^{inner}, \chi_{DPPC}^{outer}\right) = f_M\left(\chi_{DPPC}^{inner}\right) + f_M\left(\chi_{DPPC}^{outer}\right) + \Lambda(\chi_{DPPC}^{inner} - \chi_{DPPC}^{outer})^2, \quad [7]$$

where χ_{DPPC}^{inner} and χ_{DPPC}^{outer} refer to inner and outer leaflet compositions of the binary DPPC/DOPC mixture and f_M is the local leaflet free energy,

$$f_M\left(\chi_{DPPC}^{j}\right) = \chi_{DPPC}^{j}\ln\chi_{DPPC}^{j} + \left(1-\chi_{DPPC}^{j}\right)\ln\left(1-\chi_{DPPC}^{j}\right) + \mathrm{X}\chi_{DPPC}^{j}\left(1-\chi_{DPPC}^{j}\right), \quad [8]$$

that depends on leaflet composition χ_{DPPC}^{j}, for j = *inner* or *outer*.

For a binary mixture with a single compositional degree of freedom in each leaflet, the asymmetric bilayer can separate into at most three bilayer-spanning phases (two registered and one AR) with six distinct leaflet phase compositions. For fixed values of X and Λ, these were determined by numerical minimization of Eqs. **7** and **8** subject to conservation of leaflet area and composition as described in ref. 13.

Data, Materials, and Software Availability. All study data are included in the article and/or *SI Appendix*.

ACKNOWLEDGMENTS. We thank John Williamson, Sylvio May, Gerald Feigenson, and Erwin London for insightful discussions. This work was supported by NSF Grant MCB–1817929 (to F.A.H.). T.A.E. acknowledges the financial support from São Paulo Research Foundation FAPESP (2022/04046-4 and 2023/05540-5).

Author affiliations: [a]Department of Chemistry, University of Tennessee, Knoxville, TN 37996; and [b]Department of Molecular Biology and Genetics, Cornell University, Ithaca, NY 14853

1. J. H. Lorent *et al.*, Plasma membranes are asymmetric in lipid unsaturation, packing and protein shape. *Nat. Chem. Biol.* **16**, 644–652 (2020).
2. E. London, Membrane structure-function insights from asymmetric lipid vesicles. *Acc. Chem. Res.* **52**, 2382–2391 (2019).
3. I. Levental, K. R. Levental, F. A. Heberle, Lipid rafts: Controversies resolved, mysteries remain. *Trends Cell Biol.* **30**, 341–353 (2020).
4. R. Raghupathy *et al.*, Transbilayer lipid interactions mediate nanoclustering of lipid-anchored proteins. *Cell* **161**, 581–594 (2015).
5. M. B. Stone, S. A. Shelby, M. F. Núñez, K. Wisser, S. L. Veatch, Protein sorting by lipid phase-like domains supports emergent signaling function in b lymphocyte plasma membranes. *Elife* **6**, e19891 (2017).
6. T. Harder, M. Kuhn, Selective accumulation of raft-associated membrane protein LAT in T cell receptor signaling assemblies. *J. Cell Biol.* **151**, 199–207 (2000).
7. G. van Meer, D. R. Voelker, G. W. Feigenson, Membrane lipids: Where they are and how they behave. *Nat. Rev. Mol. Cell Biol.* **9**, 112–124 (2008).
8. G. W. Feigenson, Phase behavior of lipid mixtures. *Nat. Chem. Biol.* **2**, 560–563 (2006).
9. T. Y. Y. Wang, J. R. Silvius, Cholesterol does not induce segregation of liquid-ordered domains in bilayers modeling the inner leaflet of the plasma membrane. *Biophys. J.* **81**, 2762–2773 (2001).
10. F. A. Heberle, G. W. Feigenson, Phase separation in lipid membranes. *Cold Spring Harb. Perspect. Biol.* **3**, 1–13 (2011).
11. J. Reinhard *et al.*, Remodeling of yeast vacuole membrane lipidomes from the log (one phase) to stationary stage (two phases). *Biophys. J.* **122**, 1043–1057 (2023).
12. S. May, Trans-monolayer coupling of fluid domains in lipid bilayers †. *Soft Matter* **5**, 3148–3156 (2009).
13. A. J. Wagner, S. Loew, S. May, Influence of monolayer–monolayer coupling on the phase behavior of a fluid lipid bilayer. *Biophys. J.* **93**, 4268–4277 (2007).
14. G. G. Putzel, M. Schick, Phase behavior of a model bilayer membrane with coupled leaves. *Biophys. J.* **94**, 869–877 (2008).
15. J. J. Williamson, P. D. Olmsted, Effects of passive phospholipid flip-flop and asymmetric external fields on bilayer phase equilibria. *Biophys. J.* **115**, 1956–1965 (2018).
16. F. A. Heberle, J. T. Buboltz, D. Stringer, G. W. Feigenson, Fluorescence methods to detect phase boundaries in lipid bilayer mixtures. *Biochim. Biophys. Acta* **1746**, 186–192 (2005).
17. T. M. Konyakhina, J. Wu, J. D. Mastroianni, F. A. Heberle, G. W. Feigenson, Phase diagram of a 4-component lipid mixture: DSPC/DOPC/POPC/chol. *Biochim. Biophys. Acta* **1828**, 2204–2214 (2013).
18. R. S. Petruzielo, F. A. Heberle, P. Drazba, J. Katsaras, G. W. Feigenson, Phase behavior and domain size in sphingomyelin-containing lipid bilayers Author' s personal copy. *Biochim. Biophys. Acta* **1828**, 1302–1313 (2013).
19. T. A. Enoki, F. A. Heberle, G. W. Feigenson, FRET detects the size of nanodomains for coexisting liquid-disordered and liquid-ordered phases. *Biophys. J.* **114**, 1921–1935 (2018).
20. F. A. Heberle *et al.*, Bilayer thickness mismatch controls domain size in model membranes. *J. Am. Chem. Soc.* **135**, 6853–6859 (2013).
21. F. A. Heberle *et al.*, Direct label-free imaging of nanodomains in biomimetic and biological membranes by cryogenic electron microscopy. *Proc. Natl. Acad. Sci. U.S.A.* **117**, 19943–19952 (2020).
22. C. E. Cornell, A. Mileant, N. Thakkar, K. K. Lee, S. L. Keller, Direct imaging of liquid domains in membranes by cryo-electron tomography. *Proc. Natl. Acad. Sci. U.S.A.* **117**, 19713–19719 (2020).
23. T. A. Enoki, G. W. Feigenson, Asymmetric bilayers by hemifusion: Method and leaflet behaviors. *Biophys. J.* **117**, 1037–1050 (2019).
24. T. A. Enoki, G. W. Feigenson, Improving our picture of the plasma membrane: Rafts induce ordered domains in a simplified model cytoplasmic leaflet. *Biochim. Biophys. Acta Biomembr.* **1864**, 183995 (2022).
25. T. A. Enoki, J. Wu, F. A. Heberle, G. W. Feigenson, Investigation of the domain line tension in asymmetric vesicles prepared via hemifusion. *Biochim. Biophys. Acta Biomembr.* **1863**, 183586 (2021).
26. T. A. Enoki, J. Wu, F. A. Heberle, G. W. Feigenson, Dataset of asymmetric giant unilamellar vesicles prepared via hemifusion: Observation of anti-alignment of domains and modulated phases in asymmetric bilayers. *Data Brief* **35**, 106927 (2021).
27. H. L. Scott *et al.*, Model membrane systems used to study plasma membrane lipid asymmetry. *Symmetry (Basel)* **13**, 1356 (2021).
28. G. W. Feigenson, T. A. Enoki, Nano-scale domains in the plasma membrane are like macroscopic domains in asymmetric bilayers. *Biophys. J.* **122**, 925–930 (2023).
29. M. L. Schmidt, L. Ziani, M. Boudreau, J. H. Davis, Phase equilibria in DOPC/DPPC: Conversion from gel to subgel in two component mixtures. *J. Chem. Phys.* **131**, 175103 (2009).
30. T. J. Larocca *et al.*, Proving lipid rafts exist: Membrane domains in the prokaryote borrelia burgdorferi have the same properties as eukaryotic lipid rafts. *PLoS Pathog.* **9**, e1003353 (2013).
31. H. T. Cheng, E. London, Preparation and properties of asymmetric large unilamellar vesicles: Interleaflet coupling in asymmetric vesicles is dependent on temperature but not curvature. *Biophys. J.* **100**, 2671–2678 (2011).
32. S. Chiantia, E. London, Acyl Chain length and saturation modulate interleaflet coupling in asymmetric bilayers: Effects on dynamics and structural order. *Biophys. J.* **103**, 2311–2319 (2012).
33. M. Doktorova *et al.*, Preparation of asymmetric phospholipid vesicles for use as cell membrane models. *Nat. Protoc.* **13**, 2086–2101 (2018).
34. Q. Wang, E. London, Lipid structure and composition control consequences of interleaflet coupling in asymmetric vesicles. *Biophys. J.* **115**, 664–678 (2018).
35. M. Doktorova, I. Levental, F. A. Heberle, Seeing the membrane from both sides now: Lipid asymmetry and its strange consequences. *Cold Spring Harb. Perspect. Biol.*, 10.1101/cshperspect.a041393 (2023).
36. G. W. Feigenson, J. Huang, T. A. Enoki, An unexpected driving force for lipid order appears in asymmetric lipid bilayers. *J. Am. Chem. Soc.* **145**, 21717–21722 (2023).
37. M. D. Collins, Interleaflet coupling mechanisms in bilayers of lipids and cholesterol. *Biophys. J.* **94**, L32–L34 (2008).
38. H. J. Risselad, S. J. Marrink, The molecular face of lipid rafts in model membranes. *Proc. Natl. Acad. Sci. U.S.A.* **105**, 17367–17372 (2008).
39. M. C. Blosser, A. R. Honerkamp-Smith, T. Han, M. Haataja, S. L. Keller, Transbilayer colocalization of lipid domains explained via measurement of strong coupling parameters. *Biophys. J.* **109**, 2317–2327 (2015).
40. Q. Lin, E. London, Ordered raft domains induced by outer leaflet sphingomyelin in cholesterol-rich asymmetric vesicles. *Biophys. J.* **108**, 2212–2222 (2015).
41. C. Wan, V. Kiessling, L. K. Tamm, Coupling of cholesterol-rich lipid phases in asymmetric bilayers. *Biochemistry* **47**, 2190–2198 (2008).
42. M. D. Collins, S. L. Keller, Tuning lipid mixtures to induce or suppress domain formation across leaflets of unsupported asymmetric bilayers. *Proc. Natl. Acad. Sci. U.S.A.* **105**, 124–128 (2008).
43. F. A. Heberle *et al.*, Subnanometer structure of an asymmetric model membrane: Interleaflet coupling influences domain properties. *Langmuir* **32**, 5195–5200 (2016).
44. G. W. Feigenson, Phase boundaries and biological membranes. *Annu. Rev. Biophys. Biomol. Struct.* **36**, 63–77 (2007).
45. D. Marquardt *et al.*, 1H NMR shows slow phospholipid flip-flop in gel and fluid bilayers. *Langmuir* **33**, 3731–3741 (2017).
46. T. J. McIntosh, S. A. Simon, R. C. MacDonald, The organization of n-alkanes in lipid bilayers. *Biochim Biophys Acta* **597**, 445–463 (1980).
47. T. A. Harroun, J. Katsaras, S. R. Wassall, Cholesterol is found to reside in the center of a polyunsaturated lipid membrane. *Biochemistry* **47**, 7090–7096 (2008).
48. D. Marquardt *et al.*, Lipid bilayer thickness determines cholesterols location in model membranes. *Soft Matter.* **12**, 9417–9428 (2016).
49. T. Baumgart *et al.*, Large-scale fluid/fluid phase separation of proteins and lipids in giant plasma membrane vesicles. *Proc. Natl. Acad. Sci. U.S.A.* **104**, 3165–3170 (2007).
50. I. Levental *et al.*, Cholesterol-dependent phase separation in cell-derived giant plasma-membrane vesicles. *Biochem. J.* **424**, 163–167 (2009).
51. D. Lingwood, J. Ries, P. Schwille, K. Simons, Plasma membranes are poised for activation of raft phase coalescence at physiological temperature. *Proc. Natl. Acad. Sci. U.S.A.* **105**, 10005–10010 (2008).
52. P. Sengupta, A. Hammond, D. Holowka, B. Baird, Structural determinants for partitioning of lipids and proteins between coexisting fluid phases in giant plasma membrane vesicles. *Biochim. Biophys. Acta Biomembr.* **1778**, 20–32 (2008).

53. H. J. Kaiser *et al.*, Order of lipid phases in model and plasma membranes. *Proc. Natl. Acad. Sci. U.S.A.* **106**, 16645–16650 (2009).
54. A. D. Skinkle, K. R. Levental, I. Levental, Cell-derived plasma membrane vesicles are permeable to hydrophilic macromolecules. *Biophys. J.* **118**, 1292–1300 (2020).
55. S. Kakuda, P. Suresh, G. Li, E. London, Loss of plasma membrane lipid asymmetry can induce ordered domain (raft) formation. *J. Lipid Res.* **63** (2022).
56. M. Doktorova, J. L. Symons, I. Levental, Structural and functional consequences of reversible lipid asymmetry in living membranes. *Nat. Chem. Biol.* **16**, 1321–1330 (2020).
57. J. Steinkühler, P. De Tillieux, R. L. Knorr, R. Lipowsky, R. Dimova, Charged giant unilamellar vesicles prepared by electroformation exhibit nanotubes and transbilayer lipid asymmetry. *Sci. Rep.* **8**, 11838 (2018).
58. T. R. Shaw *et al.*, Chemical potential measurements constrain models of cholesterol-phosphatidylcholine interactions. *Biophys. J.* **122**, 1105–1117 (2023), 10.1016/J.BPJ.2023.02.009.
59. J. T. Buboltz, G. W. Feigenson, A novel strategy for the preparation of liposomes: Rapid solvent exchange. *Biochim. Biophys. Acta Biomembr.* **1417**, 232–245 (1999).
60. M. I. Angelova, D. S. Dimitrov, Liposome electroformation. *Faraday Discuss. Chem. Soc.* **81**, 303 (1986).